ASIA-PACIFIC JOURNAL OF CHEMICAL ENGINEERING
Asia-Pac. J. Chem. Eng. (2012)
Published online in Wiley Online Library
(wileyonlinelibrary.com) DOI: 10.1002/apj.1702

Research article

CFD analysis to study the effect of design variables on the particle cut size in hydrocyclones

J. A. Delgadillo, G. Rosales-Marin, C. Perez-Alonso and C. Ojeda*

Facultad de Ingenieria-Instituto de Metalurgia, Universidad Autonoma de San Luis Potosi, San Luis Potosi, San Luis Potosi, Mexico

Received 19 June 2012; Revised 25 October 2012; Accepted 5 November 2012

ABSTRACT: The modification of hydrocyclone geometry changes the dynamics of the flow, so the particle cut size is affected. Computational fluid dynamics was applied to predict particle classification according to size. Fluent code was used to perform computer simulations for five different hydrocyclone geometries using large eddy simulation and volume of fluid models. The sensitivity to computed modifications in particle classification was evaluated by changing basic design variables, such as spigot diameter, vortex finder diameter, and cone angle. The results show that the particle cut size can be predicted for changes in geometric configuration for a wide range of slurry concentration with a small degree of error using computational fluid dynamics. The error can be attributed to the absence of particle–particle and fluid–particle interaction modeling. However, this assumption is known to be valid only for diluted slurries and some regions within the hydrocyclone. As soon as the particles enter the system, most of them are located within the walls, creating diluted slurry conditions in the main core of the hydrocyclone. The computed results for more concentrated slurries were therefore close to the experimental cut-size values. In all cases, the particle cut size was predicted successfully. Therefore, the evaluation of changes in the standard geometry to manipulate the dynamics and achieve the desired particle cut size becomes possible.

KEYWORDS: hydrocyclone; cut size; particle classification; CFD

INTRODUCTION

The hydrocyclone, widely used in industry, consists of a cylindrical upper body with a central tube called a vortex finder and a conical lower body with a discharge tube called a spigot. The slurry is fed into the tangential inlet, creating a swirling flow and generating a high centrifugal field in the cylindrical section. The conical section restricts the flow downward, causing part of the flow to reverse and exit through the vortex finder. The high centrifugal field accelerates coarse particles toward the wall. In turn, these particles become trapped in the downward flow and are discharged through the spigot. The finer particles remain in the central column of upward flow, which carries these particles and discharges them through the vortex finder. Because the discharge outlets are open to the atmosphere, a low-pressure air core forms along the central axis. The dynamics of this swirl flow and the presence of three phases make modeling a challenge. In the early 1970s, empirical models were used for hydrocyclone prediction. However, with the development of computing power and codes to solve fluid dynamics, direct solution of the rigorous flow problem has become possible.

In the past 20 years, computational fluid dynamics (CFD) has been used in the metallurgical field;[1–3] however, in the mining and mineral processing industry, primarily empirical models have been developed.[4,5] These empirical models quantify the misclassification of particles and predict the operational characteristics. Empirical models are easy to apply to a specific operation; particle size classifications can be predicted using the dimensions of the hydrocyclone and constants related to the characteristics of the slurry. The data collected under a variety of operating conditions are usually correlated with empirical expressions using the multiple linear regression method.

The main disadvantage of this type of modeling is that when the constants of the model are calibrated for a specific operating condition, the same model cannot be used to predict new scenarios greatly different from the calibrated conditions. Furthermore, these models do not explain why some fine particles are guided to the coarse stream outlet and why some of the feed particles are directly guided to the fine stream outlet. Understanding the dynamics of fluid and

**Correspondence to*: Jose A. Delgadillo, Facultad de Ingenieria-Instituto de Metalurgia, Universidad Autonoma de San Luis Potosi, San Luis Potosi, San Luis Potosi, Mexico. E-mail: jose.delgadillo@uaslp.mx

particle motion is essential to improve the performance of the hydrocyclone, and empirical models are not capable of providing such information.

Because empirical models cannot explain the internal mechanics of fluid flow, models based on the physics of the flow can be used. Fluid dynamics provides a fundamental approach to solve the internal flow in hydrocyclones for any variation in geometry or flow conditions. In this work, a CFD analysis of the design variables for particle classification is presented, and the lack of accuracy of the solid split prediction is discussed.

Fluid dynamics models have three main parts: the mass balance, the momentum balance, and the turbulence effect. The mass balance is described using the continuity equation, the momentum balance is explained using the Navier–Stokes equations, and the turbulence effect is described with a turbulence-closure model. The continuity equation and Navier–Stokes equations are nonlinear partial differential equations in three dimensions and thus require great computational effort. The solution of these equations falls under the discipline called CFD.

The three phases must be simulated to fully describe the classification of hydrocyclones. The water phase is simulated with the Navier–Stokes equations with an additional model to describe the turbulence effect. Next, the diameter and profile of the air core must be described, especially for large hydrocyclones where the area occupied by the air core significantly modifies the water-split ratio. The description of the particle trajectory represents a great challenge and requires additional modeling.

Several authors[6–11,23] have demonstrated that the large eddy simulation (LES) model is the most adequate approach compared with other available models to simulate turbulence closure in hydrocyclones. The LES model performs remarkably well without a prohibitively high computational cost. However, the computationally more expensive LES provides the best solution for hydrocyclone turbulence, which will potentially impact the separation efficiency calculations.

The air core is the most important internal structure generated inside the hydrocyclone. The volume of fluid (VOF) model with the LES model for turbulence closure has been demonstrated[6–10] to predict the air core formation successfully. Narasimha *et al.*[10] showed that the VOF model with LES can predict the air core for 75 and 101-mm hydrocyclones. These authors conclude that CFD can be used to describe the air core shape and diameter for various operational conditions. Delgadillo and Rajamani[9] showed that a geometric change in the hydrocyclone modifies the structure of the air core, but the modification can be successfully predicted by LES–VOF models.

The LES model with the VOF model can successfully predict the fluid flow and air core structure for any given geometry and operational condition, as has been very well demonstrated. After establishing the flow field of water and the air core, the next step is to track the pathways of solid particles of different sizes entering the inlet of the hydrocyclone. Tracking each and every particle through the hydrocyclone is an enormous computational task. However, the particles can be handled as a discrete phase using a Lagrangian formulation. This approach is not the best for describing particle trajectories, but a Lagrangian formulation has been demonstrated to provide an acceptable prediction with a degree of error by several authors.[5–7,12–15] Lagrangian formulation is a force balance that includes the forces acting on the particle as well as the dispersion due to turbulent eddies present in the continuous phase. The limitation of this approach is the volume fraction of particles that can be handled. When particles are fed in the fluid phase, the properties of the fluid change. Therefore, it is necessary to assume that the fluid is diluted sufficiently so that the effect is not significant. Nevertheless, even if the feed concentration is high, particles quickly migrate to the wall, creating a condition wherein the body of the hydrocyclone becomes diluted. In this region, it can be assumed to be a low particle concentration problem in which a Lagrangian formulation is suitable, but in the spigot region, this assumption is not valid because the concentration is not diluted. The change in the slurry concentration within the domain modifies the viscosity, damping the CFD solution and creating large deviations from the experimental data in some cases. This problem has not been addressed and must be included in a CFD simulation to improve the accuracy of solid prediction. Furthermore, the particle shape has shown an effect on classification.[22] Kashiwaya *et al.*[22] demonstrated that the recovery of coarse particles is a function of the particle shape when the drag force is modified as the ratio of the particle diameter to thickness increases. This variation is not considered in the simulation where spherical particles are used in the computations.

CFD MODELS

To model the dynamics of flow for any system, the governing equations are needed. The mass balance and momentum balance are the main parts of this modeling, in addition to the models that are necessary to describe turbulent transport, interface characteristics, and particle trajectory. A filtering operation decomposes the velocity into the sum of a resolved (larger scale) component and a residual (subgrid scale) component. The filtering operation is applied to the Navier–Stokes equations resulting in Eqns (1) and (2). The mass balance is described by the continuity equation shown in Eqn (1) and the momentum balance in Eqn (2).

DOI: 10.1002/apj

$$\frac{\partial \rho}{\partial t} + \rho \frac{\partial \bar{u}_i}{\partial x_i} = 0 \quad (1)$$

$$\frac{\partial \bar{u}_i}{\partial t} + \frac{\partial \left(\bar{u}_i \bar{u}_j\right)}{\partial x_j} = -\frac{1}{\rho}\frac{\partial \bar{p}}{\partial x_i} + \frac{\partial}{\partial x_j}\left(\mu \frac{\partial \bar{u}_i}{\partial x_j}\right) - \frac{\partial \tau_{ij}{}^{\mathrm{sgs}}}{\partial x_j} + g_i \quad (2)$$

The flow in hydrocyclones can be described using Eqns (1) and (2). These equations can be solved only by numerical methods. The LES approach has been used with great success compared with available turbulence models and has been effective for solving the fluid flow in hydrocyclones.[6–8,10,11,16,17] In LES, the subgrid scale tensor $\left(\tau_{ij}^{\mathrm{sgs}}\right)$ contains all the turbulence fluctuations, as described in Eqn (2). The turbulent viscosity (μ_t) is modeled by the Smagorinsky–Lilly model.[18]

$$\tau_{ij}^{\mathrm{sgs}} = -\mu_t\left(\frac{\partial \bar{u}_i}{\partial x_j} + \frac{\partial \bar{u}_j}{\partial x_i}\right) \quad (3)$$

Next, the eddy viscosity of the residual motions, μ_t, must be modeled. The standard model for τ_{ij}^{sgs} proposed by Smagorinsky[18] relates the eddy viscosity to the filter width, but this standard model does not include the effect of molecular viscosity, which has a significant effect on the flow close to the walls. To include molecular viscosity, Yakhot *et al.*[24] introduced the renormalization group (RNG) formulation, in which molecular viscosity is included to give a better description of the turbulence at the walls. The turbulent viscosity is defined as the difference between the effective viscosity and molecular viscosity, as shown in Eqn (4).

$$\mu_t = \mu_{\mathrm{eff}} - \mu \quad (4)$$

According to Yakhot *et al.*,[24] the experimental data available for the subgrid scale motions show that the effective viscosity conforms to Eqn (5). The Heaviside function $H(x)$ is solved when Eqns (6) and (7) produce a finite value in the positive range of numbers.

$$\mu_{\mathrm{eff}} = \mu[1 + H(x)]^{1/3} \quad (5)$$

$$x = \frac{\mu_s^2 \mu_{\mathrm{eff}}}{\mu^3} - C \quad (6)$$

$$\mu_{\mathrm{s}} = \left(C_{\mathrm{RNG}} V^{1/3}\right)^2 \sqrt{2\bar{S}_{ij}\bar{S}_{ij}} \quad (7)$$

where C is 100 and $H(x)$ is the Heaviside function, defined as $H(x) = x$ for $x \geq 0$ and $H(x) = 0$ for $x \leq 0$, representing the fact that when the flow is close to the wall region, the velocity is reduced. At some point, the flow becomes more laminar and reduces the effect of subgrid scale motions. When the ratio $\mu_{\mathrm{s}}^2 \mu_{\mathrm{eff}}/\mu^3$ is less than C, the flow behaves more similar to a laminar flow, and the turbulent viscosity is zero. When $\mu_{\mathrm{s}}^2 \mu_{\mathrm{eff}}/\mu^3$ is greater than C, the flow is turbulent, resulting in the Smagorinsky eddy viscosity model, which resolves the subgrid scale motions.

In addition, the air/water interface formed in the core of the hydrocyclone must be modeled. The air core structure was simulated as a free surface problem using the VOF model to describe the location of the air/water interface. The VOF model simulates the position of the interface by solving the transport equation shown in Eqn (8). The transport equation for the volume fraction of the air, α_γ, is solved, and the properties in any given cell are represented by α_γ in the air and water mixture. Therefore, for each cell of the mesh that describes the domain, the volume fraction of air and water is computed. For any property, f, of the two phases (air (1) and water (2)), the volume fraction is taken from Eqn (9).

$$\frac{\partial \alpha_\gamma}{\partial t} + u_i \frac{\partial \alpha_\gamma}{\partial x_i} = 0 \quad (8)$$

$$f = \sum_{\gamma=1}^{\gamma=2} \alpha_\gamma f_\gamma \quad (9)$$

In this manner, density and viscosity can be computed for each cell throughout the domain. The corresponding momentum equation is solved using the average density and viscosity at the interface. The resulting velocity field is shared between the two phases. The modification of the viscosity and density due to particle concentration is not included in the simulation. The error in prediction is then attributed to this lack of modeling, and a modified model is needed to cope with the interactions of fluid and particles.

After the flow field is described and the air core structure is predicted, the next step is to track the particle trajectory of different particle sizes. The particle trajectory is modeled using the Lagrangian formulation, which includes the forces acting on the particle and the prediction of the dispersion due to turbulence eddies present in the continuous phase. The force balance over a particle, in a Lagrangian reference frame for unsteady flows, is the sum of drag and gravitational forces acting on the particle, which can be written as shown in Eqn (10).

$$\frac{\mathrm{d}u_{\mathrm{P}}}{\mathrm{d}t} = F_{\mathrm{D}}(u - u_{\mathrm{P}}) + g\frac{(\rho_{\mathrm{P}} - \rho)}{\rho_{\mathrm{P}}} \quad (10)$$

where

$$F_{\mathrm{D}} = \frac{18\mu}{\rho_{\mathrm{p}} d_{\mathrm{p}}^2}\frac{C_{\mathrm{D}}\mathrm{Re}}{24} \quad (11)$$

$$\mathrm{Re} = \frac{\rho d_{\mathrm{p}} \left|u_{\mathrm{p}} - u\right|}{\mu} \quad (12)$$

DOI: 10.1002/apj

$$C_D = a_1 + \frac{a_2}{Re} + \frac{a_3}{Re^2} \quad (13)$$

where a_1, a_2, and a_3 are constants that apply to smooth spherical particles over several ranges of Re as given by Morsi and Alexander.[21] The particles are dispersed because of the turbulence in the continuous phase. The turbulence creates eddies that move the particles in a random order, modifying their trajectory. The effect of turbulence can be modeled by integrating the time scale that describes the time spent by the turbulent motion along the particle path, ds. Equation (14) shows the integration and the time scale (T) resulting from such an integration. T is the integral time proportional to the particle dispersion rate. Therefore, marginal values of T denote more turbulent motions in the flow, increasing the deviation of the particle trajectory.

$$T = \int_0^\infty \frac{u'_p(t)u'_p(t+s)}{\vec{u}'_p{}^2} ds \quad (14)$$

These three models can describe the effect of design variables on the cut-size behavior in hydrocyclones. The description of the water, air core, and particles in a phenomenological model can be used to describe the fluid dynamics for hydrocyclones under a wide range of operational conditions. The principal contribution of such a model is the capability of CFD to study and explore novel designs of hydrocyclones. Changes in the standard geometry of hydrocyclones to manipulate the dynamics and achieve the desired cut size at a very low exploration cost can be evaluated.

RESULTS AND DISCUSSION

Published experimental data were used to validate the simulation results.[16,19,20] Table 1 shows the five hydrocyclone geometries studied in this work. The experimental data were used to verify the effect of spigot diameter, vortex finder diameter, and cone angle on particle classification behavior. The classification cut size was used to validate the simulated results, defined as the percentage of the particles guided to the underflow for each size.

Predicting measured velocity profiles is the most universal method of verification, although predicting Reynolds's stresses is more advanced for characterizing modeled turbulence if such a measurement is available. In this paper, velocity profiles were predicted for each geometry by using the LES and VOF models.

Under each set of conditions, the simulation was run until a steady state was reached. A real time of 2 s was simulated with a time step of 0.0005 s. The simulations were performed on a dual CPU Xeon 2.4 GHz workstation where a typical simulation required 168 h to complete. The boundary conditions imposed on the air core were a pressure outlet of 0 Pa at the overflow and underflow using the semi-implicit method for pressure-linked equations method for pressure–velocity coupling. The standard wall function was used for the solution at the wall.

The flow can be described in the three spatial components: axial, tangential, and radial velocities. For this analysis, only the axial and tangential components were considered. The radial component is the smallest in magnitude of the three components; additionally, the radial component is difficult to measure. Because experimental data were not available, the radial component was not considered in the validation.

To validate the velocity field within the hydrocyclones (G1–G5), the location of a plane just below the vortex finder (60 mm from the top) was chosen for validation. In Fig. 1, the axial and tangential velocity profiles for geometry G1 are shown. In the LES model, a constant, C_{rng}, must be calibrated for the flow field in hydrocyclones. Using the geometry G1, we present a variation of C_{rng}. The velocity profiles give a better proof for the selection of the subgrid scale constant. The simulated results for each variation of C_{rng} were compared with experimental data in the axial and tangential components.

The velocity profiles are predicted with the range of C_{rng} values presented. Therefore, the operational condition predictions with a C_{rng} value of 0.157 are found

Table 1. Geometry of the hydrocyclones, all dimensions in mm.

	Hydrocyclones				
	G1[16]	G2[20]	G3[20]	G4[20]	G5[20]
Diameter	75	75	75	75	75
Diameter of the inlet	25	25	25	25	25
Diameter of the vortex finder	25	25	25	22	25
Diameter of the spigot	12.5	15	16	11	11
Length of the vortex finder	50	50	50	50	50
Length of cylindrical section	75	75	75	75	75
Length of the conical section	186	179	176	190	211
Included angle	20°	20°	20°	20°	15°

DOI: 10.1002/apj

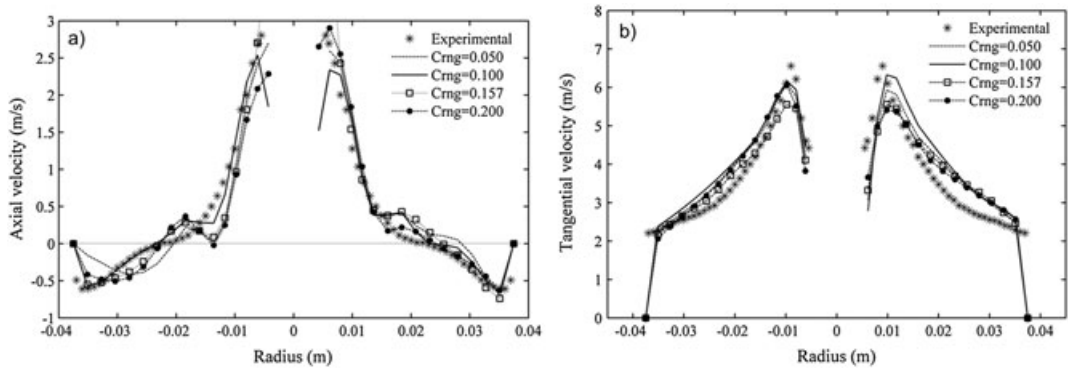

Figure 1. (a) Axial and (b) tangential velocity predictions for geometry G1 at 60 mm from the top. Experimental data from Hsieh.[16]

acceptable, and 0.157 is the default value for the C_{rng} constant[18] used in all simulations.

The increase of the spigot diameter creates a reduction in the tangential velocity. The capability of LES to capture such changes is shown in this paper. The predicted velocity profiles are shown in Figs 2 and 3. The velocity profile results are shown only for the water phase and are truncated in the air section because there is no experimental information to validate such results. The velocity profiles are shown in Fig. 3 where the velocity profiles were accurately predicted. The deviations, where the maximum points were missed, are presented in Fig. 3(a).

The velocity predictions are in agreement with the experimental data. LES predicts the change in the velocity profiles. The modification of the vortex finder diameter changes the magnitude of the velocity components. The tangential velocity increases, whereas the axial velocity magnitude decreases. The reduction of the vortex finder diameter causes the decrease in the axial velocity. LES computation adapts successfully to the change in the vortex finder diameter (Fig. 4).

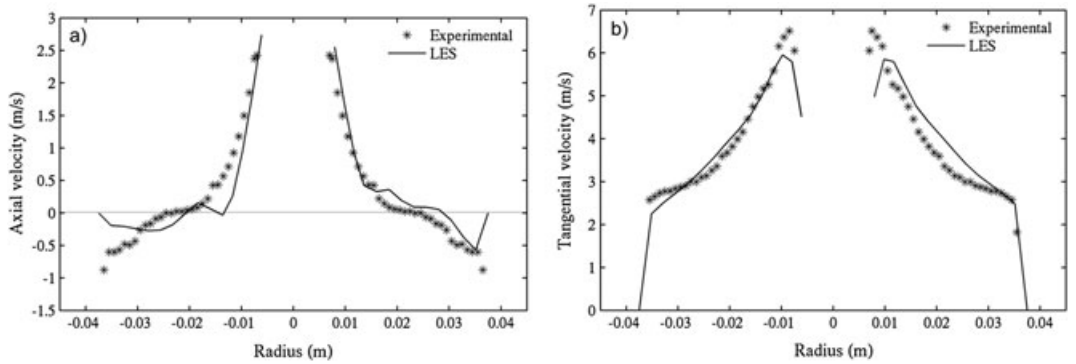

Figure 2. (a) Axial and (b) tangential velocity predictions for geometry G2 at 60 mm from the top. Experimental data from Monredon.[20]

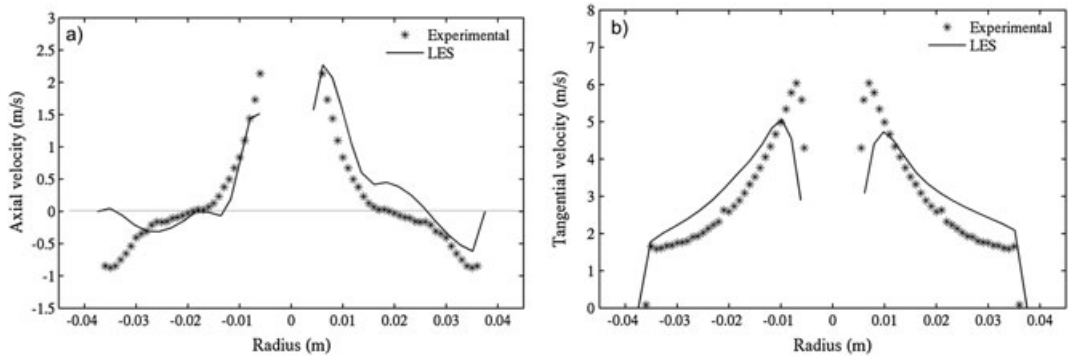

Figure 3. (a) Axial and (b) tangential velocity predictions for geometry G3 at 60 mm from the top. Experimental data from Monredon.[20]

DOI: 10.1002/apj

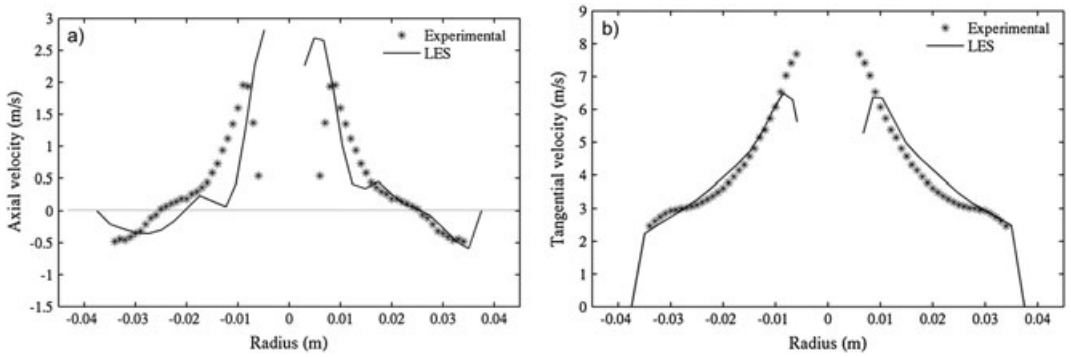

Figure 4. (a) Axial and (b) tangential velocity predictions for geometry G4 at 60 mm from the top. Experimental data from Monredon.[20]

Figure 5 shows the computed velocity profiles for a modification of the cone angle. The velocity profiles were predicted very well. The axial and tangential velocities were modified by the increment of the hydrocylone volume due to the reduction of the cone angle. The LES model adjusts to the change in the dynamics without modification of the simulation parameters. Once the velocity profiles are validated, the particle trajectory can be simulated.

Once the velocity field is predicted, the particles can be injected to predict the trajectory and the classification for each particle size. Particles are treated as a discrete phase that does not interact with the fluid. The limitation of computer power allows only this approach to handle particles. The particle trajectory is computed at the end of each time step after the fluid velocity field is updated. The classification experiments were conducted with a slurry of limestone (density 2700 kg/m^3) at different concentrations.

The particles were injected through the surface at the inlet for each size class, and exit via the underflow or overflow streams was tracked. An average of 1500 particles was injected to produce a converged size classification curve. These calculations are independent of the velocity field calculation. The boundary conditions imposed on the discrete phase were that the particles can escape only through the overflow or underflow and must be reflected at the walls of the hydrocyclone body.

The split ratio for each size fraction was calculated from samples of the overflow and underflow streams. Knowing the feed size distribution and solid split ratio, we can calculate the size distributions of overflow and underflow. The percentage of solids for each stream was computed from the split ratio for each size fraction. Table 2 shows the estimation of the mass balance for different geometries and the solid concentration where *Exp* is the experimental value, *Sim* is the simulated result, *Error* is the difference between experimental and simulated values divided by the experimental value, and D_{50} is the hydrocyclone cut size in micrometers. A combination of 13 cases is used to describe the effect of the geometry on particle classification.

The estimation of the water split is an acceptable prediction of the experimental value, and the solid split prediction describes the experimental data with a level of error. The deviation from the experimental values can be explained because of the lack of modeling of the particle–fluid interaction. When the concentration of solids increases, this interaction becomes more important. However, as soon as the particles enter the system, most of them are located within the walls, creating a condition of diluted slurry in the main core of the hydrocyclone.

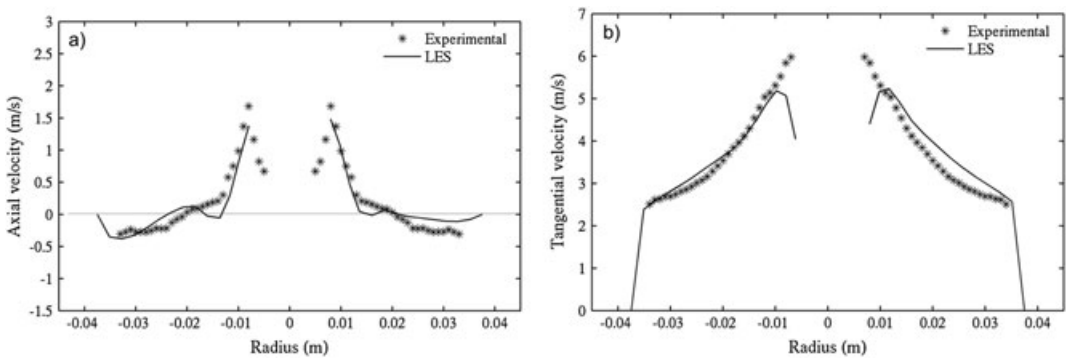

Figure 5. (a) Axial and (b) tangential velocity predictions for geometry G5 at 60 mm from the top. Experimental data from Monredon.[20]

DOI: 10.1002/apj

Table 2. Mass balance and particle cut size.

Geometry	% solids in the feed	% of solids to the underflow			% water split to the underflow			D_{50} (microns)		
		Exp	Sim	Error	Exp	Sim	Error	Exp	Sim	Error
G1	4.88	41.12	36.70	10.75	5.33	4.36	18.20	20.00	20.50	2.50
G1	10.47	44.17	39.11	11.46	4.32	5.50	27.31	20.30	21.00	3.45
G2	4.7	53.73	63.74	18.63	21.40	14.55	32.01	13.21	13.50	2.20
G2	9.88	52.91	63.53	20.07	20.65	13.94	32.49	14.00	14.20	1.43
G2	19.33	45.46	64.56	42.01	19.77	13.20	33.23	16.20	17.40	7.41
G3	4.87	55.41	57.64	4.02	24.84	14.14	43.08	12.30	13.20	7.32
G3	9.73	53.83	64.10	19.08	24.16	15.16	37.25	13.20	13.50	2.27
G4	4.74	36.25	57.06	57.41	8.87	9.21	3.83	20.30	19.30	4.93
G4	9.83	34.52	54.89	59.01	8.22	11.22	36.50	20.10	19.00	5.47
G4	19.59	28.13	56.80	101.92	7.35	10.56	43.67	25.10	23.50	6.37
G5	4.93	30.58	54.73	78.97	9.11	8.49	6.81	22.10	21.50	2.71
G5	10.84	28.58	57.73	101.99	6.93	4.41	36.36	25.10	25.00	0.40
G5	19.38	23.77	41.79	75.81	5.27	4.20	20.30	26.50	25.90	2.26

Because of this phenomenon, slurries of higher concentration can be modeled with a diluted approach.

Additionally, the error in the water split prediction greatly affects the particle classification. The error is amplified by the incorrect prediction of the flow split. Table 2 shows that the cut size (D_{50}) is well predicted with an acceptable degree of error. With the changes in geometry, the classification is modified, so the particle cut size also changes. The predicted cut sizes are in agreement with the experimental data. As the geometry changes, the prediction is accurate without any modification of the model. The other observation is the high sensitivity of the solution to captured changes in D_{50} as the particle concentration was varied. Even for slurries up to 19.59%, the prediction of the mass balance and cut size are acceptable.

The modification of the vortex finder diameter has an effect on the cut size. Figure 6 shows how the cut size varies with changes in the vortex finder diameter at different slurry concentrations. The experimental results are discrete data, whereas the simulated results are assumed to be continuous data. This assumption is applied in all the modifications explored in this paper.

Reduction of the diameter of the vortex finder increases the internal pressure of the hydrocyclone. A decrease of cut size is therefore expected. Additionally, as the concentration of the slurry increases, the pressure drop increases. The effect of the percentage of solids is well captured in Fig. 6. However, the effect of the diameter is not well differentiated because the error is greater that the real increment in cut size. This model is capable of capture modifications in particle classification as a result of changes in the vortex finder.

The other modification studied here is the effect of spigot diameter. Modification of spigot diameter is a common practice to control the cut size in industrial operations. Several modifications were tested to guarantee the precision of the results. The spigot diameter was changed at three levels, 12.5, 15.0, and 16.0 mm. The reduction of the diameter of the spigot creates a rise in the particle cut size up to 20.00 μm with geometry G1. Figure 7 shows the effect when finer cut sizes

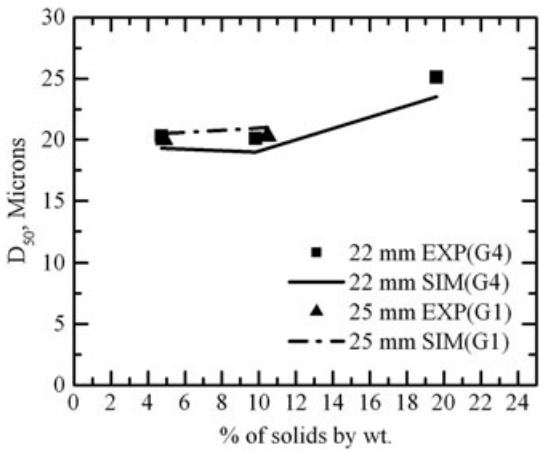

Figure 6. Hydrocyclone cut size with a change of diameter of vortex finder.

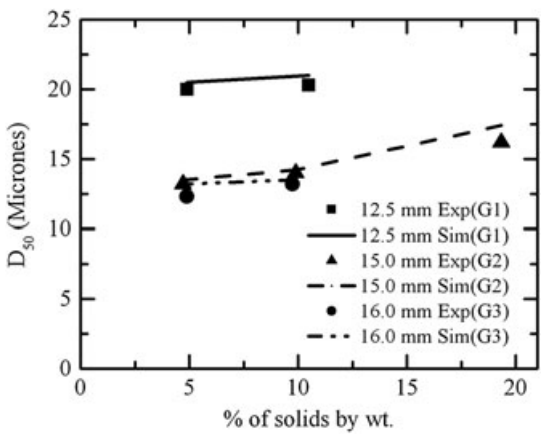

Figure 7. Modification of the cut size with a change in spigot diameter.

DOI: 10.1002/apj

up to 12.30 μm with geometry G3 are reached with a spigot diameter of 16.0 mm. The increment in the solid concentration generates an increase in cut size from 13.21 to 16.20 μm with geometry G2. In general, the predictions are close to the experimental data, and the dynamics of the process are captured.

The last change in geometry is the modification of the cone angle. Modification of the cone angle changes the split ratio and pressure drop of the system. The variation of the cone angle modifies the fluid residence time because the volume of the hydrocyclone is greatly changed by the dimensions of the cone. The modification of the residence time affects the classification process, as shown in Fig. 8.

The modification of the cone angle shows a greater impact on the operational variables. The cut size increases as the angle decreases, and the simulated results are in agreement with experimental data. The cone angle must therefore be taken into consideration for optimization of the geometry for novel designs of hydrocyclones.

The results show that particle size classification can be predicted for a concentrated slurry where the error is important, but it is a good approximation. The interaction within particles is very high, and the concentration of solids modifies the dynamics of the fluid. However, as soon as the slurry enters the system, most of the particles are driven toward the wall, and the core of the fluid remains a diluted slurry. Thus, the simulation results show some agreement with experimental data.

The cut size is predicted with some degree of error. The deviation is attributed to the interactions between the particles, which were not modeled. The predicted cut size with changes in hydrocyclone geometry demonstrates the accuracy of the particle-tracking algorithm used in this work. In Fig. 9, different particle sizes were tracked along the hydrocyclone body with geometry G5. Figure 9(a) shows tracking of the $d_p = 20$ micron particles. The particles are driven to the central core flow, with a tendency to remain in the central upward flow and eventually pass to the overflow.

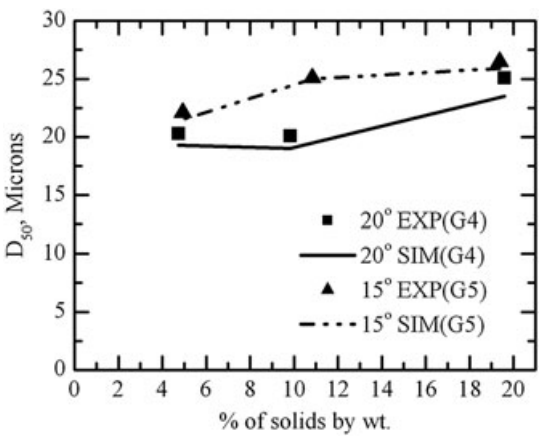

Figure 8. Change in cut size with a modification of cone angle.

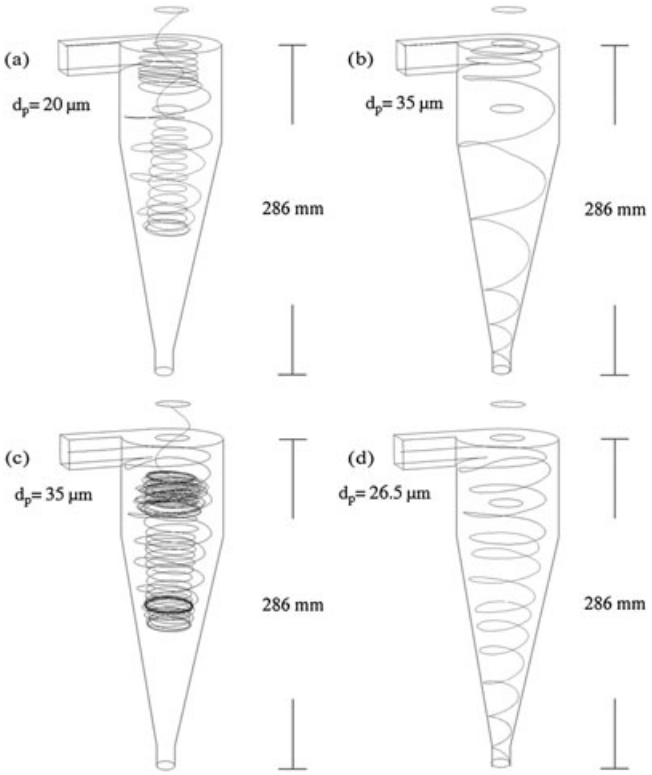

Figure 9. Computed particle trajectories in the 75-mm hydrocyclone.

Figure 9(b) and (d) shows the tracking of the $d_p = 35$ micron particles. These particles simply pass to the underflow through the outer wall region. Figure 9(c) shows tracking of the $d_p = 26.5$ micron particles, which is the cut size for this hydrocyclone. There is a 50% chance of finding a particle of this size in the underflow. These particles travel up with the central core flow and tend to remain in the core with a high recirculation in the vicinity of the upward and downward flow interface. The turbulence fluctuations affect the particle trajectory, causing the particles to either simply pass to the underflow in a tight recirculation region or discharge through the overflow.

The identification of these separation mechanisms shows the capability to predict particle classification in 75-mm hydrocyclones. The validation of particle classification is extended to larger hydrocyclones (250 mm in diameter), and this validation was published elsewhere by Delgadillo and Rajamani,[8] in which a new variable was introduced to evaluate the performance of CFD for very highly concentrated slurries.

CONCLUSIONS

Modification of the cut size due to changes in geometry and slurry concentration is captured by CFD calculations. The main limitation in these calculations is the

DOI: 10.1002/apj

lack of computer power to model particle–particle and particle–fluid interactions. This problem is overcome by the fact that the particles, as soon as they enter the body of the hydrocyclone, are headed towards the walls, but more detailed modeling is needed. This phenomenon creates a domain of diluted slurry where the interactions are not significant. Therefore, the simulation of concentrated slurries with a margin of error is possible.

Prediction of the cut size shows the performance of the particle-tracking algorithm used in this work. Additionally, the capability of CFD to predict particle classification for diluted and concentrated slurries in 75-mm hydrocyclones applying a combination of the LES, VOF, and Lagrangian formulation models for turbulence closure, air core, and particle trajectory, respectively, has been demonstrated.

Particle classification can be described accurately. The modifications in classification by geometric changes are well described. This characteristic opens a new chapter in hydrocyclone optimization. It is possible to evaluate changes in the standard geometry to manipulate the dynamics, achieving the desired particle classification. Different designs can be proposed, and the design with the required results can be tested in experimental work. Therefore, experimental testing is reduced enormously, whereas the exploration efficiency is increased.

Acknowledgement

The authors would like to thank the National Council for Science and Technology (CONACyT) for support of this work through project SEP-CONACYT No. CB-154774

NOMENCLATURE

C_D	Drag coefficient
CFD	Computational fluid dynamics
d_p	Particle diameter (m)
ds	Particle path
Exp	Experimental
F_D	Drag force (N)
g	Gravity (m/s)
$H(x)$	Heaviside function
LES	Large eddy simulation
P	Pressure
Sim	Simulated
SIMPLE	Semi-implicit method for pressure-linked equations
u_i	Velocity vector (m/s)
$\bar{u}$	Filtered velocity (m/s)
$\bar{u}'$	Subgrid-scale velocity (m/s)
u_p	Particle velocity (m/s)
VOF	Volume of fluid
x_i	Coordinate axis
γ	Volume fraction of the phase
μ_{eff}	Effective viscosity (P)
μ_T	Turbulent viscosity (P)
ρ	Density of the fluid (kg/m^3)
τ	Shear stress (Pa)
τ_{ij}^{sgs}	Residual stress tensor (Pa)

REFERENCES

[1] W. Gong, L. Zhang, M. Ode, H. Murakami, C. Zhou. *J. Min. Metall. Sect. B-Metall.*, **2010**; *46*(2)B, 153–160.
[2] Z. Meijie, G. Huazhi, H. Ao, Z. Hongxi, D. Chengji. *J. Min. Metall. Sect. B-Metall.*, **2011**; *47*(2)B, 137–147.
[3] B. Taraba, V. Slovak, Z. Michalec, J. Chura, A. Taufer. *J. Min. Metall. Sect. B-Metall.*, **2008**; *48*(1)B, 73–81.
[4] A.J. Lynch, T.C. Rao. In *Proc. 11th Int. Miner. Process. Congr.,Cagliari*, (Ed: Carta, M.), Aziende Tipografiche Bardi, Rome, **1975**; 245–260.
[5] I.R. Plitt. *CIM Bull.*, **1976**; *1*, 114–123.
[6] J.A. Delgadillo, R.K. Rajamani. *Miner. Metall. Process.*, **2005**; *22*(1), 225–232.
[7] J.A. Delgadillo, R.K. Rajamani. *Int. J. Miner. Process.*, **2005**; *77*(1), 217–230.
[8] J.A. Delgadillo, R.K. Rajamani. *Part. Sci. Technol.*, **2007**; *25*(1), 227–245.
[9] J.A. Delgadillo, R.K. Rajamani. *Int. J. Comput. Fluid Dyn.*, **2009**; *22*(1), 225–232.
[10] M. Narasimha, M.S. Brennan, M.S. Mathew, P.N. Holtham. *Int. J. Miner. Process.*, **2006**; *80*(1), 1–14.
[11] M.S. Brennan, M. Narasimha, P.N. Holtham. *Miner. Eng.*, **2007**; *20*(1), 395–406.
[12] T.C. Monredon, K.T. Hsieh, R.K. Rajamani. *Int. J. Miner. Process.*, **1992**; *35*(1), 65–83.
[13] K.U. Bhaskar, Y.R. Murthy, M.R. Raju, S. Tiwari, J.K. Srivastava, N. Ramakrishnan. *Miner. Eng.*, **2007**; *20*(1), 60–71.
[14] C.Y. Hsu, R.-M. Wu. *Drying Technol.*, **2008**; *26*(1), 1011–1017.
[15] S.M. Mousavian, A.F. Najafi. *Arch. Appl. Mech.*, **2009**; *79*(1), 1033–1050.
[16] K.T. Hsieh. Phenomenological model of the hydrocyclone, Ph.D. Thesis, University of Utah, Salt Lake City, UT. **1988**; 150.
[17] M.D. Slack, R.O. Prasad, A. Bakker, F. Boysan. *T. I. Chem. Engs.*, **2000**; *80*(1), 1098–1104.
[18] J. Smagorinsky. *J. Month. Wea. Rev.*, **1963**; *91*(1), 99–164.
[19] K.T. Hsieh, R.K. Rajamani. *AIChE J.*, **1991**; *37*(1), 735–746.
[20] T.C. Monredon. Hydrocyclone: investigation of the fluid flow model, M.S. Thesis, University of Utah, Salt Lake City, UT. **1990**; 122.
[21] S.A. Morsi, A.J. Alexander. *J. Fluid Mech.*, **1972**; *55*, 193–208.
[22] K. Kashiwaya, T. Noumachi, N. Hiroyoshi, M. Ito, M. Tsunekawa. *Powder Technol.*, **2012**; *226*, 147–156.
[23] J.A. Delgadillo, M. Al Kayed, D. Vo, A.S. Ramamurthy. *J. Min. Metall. Sect. B-Metall.*, **2012**; *48*(2)B, 197–206.
[24] A. Yakhot, A. Ozag, V. Yakhot, M. Israeli. *J. Sci. Comput.*, **1989**; *4*(2), 139–158.

DOI: 10.1002/apj